Periodic Motion for an Imperfect Solar Sail near an Asteroid

Ariadna Farrés[1]
Institute de Mathématiques de Bourgogne, Dijon 21078, France

Àngel Jorba [2]
Universitat de Barcelona, Barcelona 08007, Spain

Josep-Maria Mondelo [3]
Universitat Autónoma de Barcelona, Bellaterra 08193, Spain

Benjamin Villac [4]
University of California, Irvine, CA 92697, USA

In this paper we consider the Hill 3-body problem with the extra effect of the solar radiation pressure as a model for the motion of a solar sail close to an asteroid. To model the sail's acceleration, we include both reflectivity and absorption of the sail's material. We describe the most relevant dynamical properties of the system for different reflectivity and absorption coefficients as well as different fixed sail orientations. We show families of periodic orbits, describe how they relate to the parameters of the sail and discuss their stability.

Introduction

DUE to the small gravitational field around asteroids, solar radiation pressure (SRP) plays an important role on the dynamics around them. Hence, the systematic use of SRP to propel a satellite via specialized reflecting areas, such as solar sails, can give rise to new and interesting mission concepts. When we look at the dynamics of a satellite close to an asteroid there are three effects that must be taken into account: gravitational field, solar attraction and solar radiation pressure [1]. The first effect includes the shape and spin states of the asteroid, and it is relevant within a few radii from its surface, in what is known as the gravity regime. Far from the gravity regime, a good approximation of the asteroid's contribution to the real dynamics is obtained by considering it as a point mass. Here effects like SRP and the Sun's gravity must be taken into account. For asteroids following very eccentric orbits around the Sun, the variation of the distance to the Sun also plays an important role.

The goal of this paper is to study the dynamics of a solar sail near an asteroid. A flat solar sail will be considered, for which we will take into account not only the reflectivity but also the absorption of the sail's material [2, 3]. Our reference model will be the Augmented Hill 3-body problem, in which the asteroid is considered as a

[1]Postdoc Researcher, Institut de Mathématiques de Bourgogne - UMR 5584 CNRS, Université de Bourgogne, 9 avenue Alain Savary, 21078 Dijon, France ariadna.farres-basiana@u-bourgogne.fr

[2]Professor, Departament de Matemàtica Aplicada i Anàlisi, Universitat de Barcelona, Gran Via de les Corts Catalanes 585, 08007 Barcelona, Spain angel@maia.ub.es

[3]Associate Professor, Departament de Matemàtiques, Universitat Autónoma de Barcelona,08193 Bellaterra (Barcelona), Spain jmm@mat.uab.cat

[4]Assistant Professor, Department of Mechanical and Aerospace Engineering, University of California, Irvine, 4200 Engineering Gateway, Irvine, CA 92697, USA bvillac@uci.edu

point mass and the effect of SRP due to the solar sail is added. We will give a description of some of the most relevant dynamical properties of the system (fixed points and periodic orbits) and describe some of their possible applications to asteroid mission analysis.

It is well known that the Hill 3-body problem has two equilibrium points L_1 and L_2. When we add the effect of SRP, these two fixed points move towards the Sun. L_1 quickly moves away from the small body, while L_2 comes reasonably close to it [4, 5, 6]. For this reason, in this paper we will focus on the dynamics close to L_2 as it is more relevant for future mission applications. It is true that L_2 is in the shadow side of asteroids, and this could compromise observational missions. We will show, however, that there are many orbits on the family of orbits emanating from L_2 that spend most of their orbital period on the Sun side, making them very interesting for this kind of missions.

As we know, the linear dynamics around the displaced L_2 point is of the type center$\times$center$\times$saddle. Hence, two families of periodic orbits are born from L_2: a planar and a vertical family, each one related to the one of the two center directions. We also find two families of Halo orbits at the 1:1 resonance between the planar and vertical frequencies as we move along the planar family of periodic orbits. We will see that, as we move along the family of planar orbits, they acquire a boomerang shape that leaves the asteroid in the middle. On the other hand, the orbits on the vertical family start with an eight shape, with a large vertical amplitude. As we move along the family, they loose part of their vertical amplitude to become almost planar, and spend half of their period on the Sun side of the asteroid. Both the planar and vertical families of periodic orbits are unstable, needing a control strategy to remain on them for a long period. Finally, as we move along the family of Halo orbits, these ones come closer to the asteroid, but stay in the shadow side all the time. Nevertheless, the terminating orbits of the family are linearly stable.

When we change the orientation of the solar sail, we can displace the position of these fixed points and periodic orbits. Tilting the solar sail vertically with respect to the Sun-line will displace these invariant objects above and bellow the orbital plane, whereas tilting the solar sail horizontally with respect to the Sun-line will shift these objects to one side or another of the Sun-asteroid line. We will compute these families of equilibrium points and periodic orbits for different fixed sail orientations by means of continuation methods, and we will discuss how different reflectivity parameters for the solar sail affect their shape and properties. We will pay special attention to the terminating orbits of the families, since they come close to the small body and present interesting features for asteroid mission analysis.

The Augmented Hill for a Non-Perfectly Reflecting Solar Sail

As it has been mentioned before, to capture the dynamics of a solar sail around an asteroid we use the Augmented Hill 3-body problem (H3BP), that models the motion of two small masses (asteroid and spacecraft) which interact due to their mutual gravitational attraction and is perturbed by a distant larger body (the Sun). The Augmented H3BP also includes the effect of SRP as our satellite is propelled by a solar sail [7, 8]. Hence, in this model

the effect of the Sun is included as a uniform gravity vector field and uniform SRP, both in the horizontal direction.

We consider a rotating reference frame centered on the small body, defined such that: the x direction points from the Sun to the asteroid; the z direction is aligned with the Sun–asteroid angular velocity; and the y direction completes a positive coordinate system. We normalize the units of distance and time such that: $L = (\mu_{sb}/\mu_{sun})^{1/3}R$ and $T = 1/\omega$ respectively, where μ_{sun} is the gravitational parameter of the Sun ($\approx 1.327 \times 10^{11}$km^3/s^2), μ_{sb} is the gravitational parameter of the smaller body, R is the mean distance distance between the Sun and the asteroid, and $\omega = \sqrt{\mu_{sun}/R^3}$ is the angular velocity. Using these normalized units, the equations for the Augmented Hill Three Body Problem (AH3BP) for a solar sail [5, 6] are:

$$\begin{aligned} \ddot{X} - 2\dot{Y} &= -\frac{X}{r^3} + 3X + a_x, \\ \ddot{Y} + 2\dot{X} &= -\frac{Y}{r^3} + a_y, \\ \ddot{Z} &= -\frac{Z}{r^3} - Z + a_z, \end{aligned} \tag{1}$$

where (X, Y, Z) denotes the position of the solar sail in the rotating frame, $r = \sqrt{X^2 + Y^2 + Z^2}$ is the distance between the solar sail and the center of the asteroid, and $\mathbf{a_{sail}} = (a_x, a_y, a_z)$ is the acceleration given by the solar sail.

To model the acceleration of the solar sail we use the simplified model for a non-perfectly reflecting (SNPR) solar sail from [3], which only takes into account absorption and reflection of the sail material: if we denote the absorption coefficient as a and the reflectivity coefficient as ρ, we have $a + \rho = 1$. Besides, the force due to absorption and reflection is given by $\mathbf{F_a} = PA\langle \mathbf{r_s}, \mathbf{n}\rangle \mathbf{r_s}$ and $\mathbf{F_r} = 2PA\langle \mathbf{r_s}, \mathbf{n}\rangle^2 \mathbf{n}$ respectively. In the previous expressions, $P = P_0(R_0/R)^2$ is the SRP magnitude at a distance R from the Sun ($P_0 = 4.563\mu$N/m^2, the SRP magnitude at 1AU and $R_0 = 1$AU), A is the area of the solar sail, $\mathbf{r_s}$ is the direction of SRP and $\mathbf{n}$ is the normal direction to the surface of the sail. Hence, the acceleration for the SNPR solar sail is given by:

$$\mathbf{a_{sail}} = \frac{2PA}{m}\langle \mathbf{r_s}, \mathbf{n}\rangle \left(\rho\langle \mathbf{r_s}, \mathbf{n}\rangle \mathbf{n} + \frac{1}{2}(1-\rho)\mathbf{r_s} \right). \tag{2}$$

Notice that $\rho = 1$ corresponds to a perfectly reflecting solar sail, and $\rho = 0$ to a perfect solar array where the absorption of the solar panels is the only effect. According to [3], a solar sail with a highly reflective aluminum-coated side has an estimated value of $\rho \approx 0.88$. Nevertheless, in this paper we present a comparative result of the dynamical properties of a solar sail for different values for ρ.

Observe that, in the rotating reference frame, $\mathbf{r_s} = (1, 0, 0)$. We will parametrize the normal direction to the surface of the sail using two angles α, δ, representing the horizontal and vertical displacement with respect to $\mathbf{r_s}$: $\mathbf{n} = (\cos\alpha\cos\delta, \sin\alpha\cos\delta, \sin\delta)$. As the sail cannot point towards the Sun, we have that $\alpha, \delta \in [-\pi/2, \pi/2]$. Finally, the efficiency of our solar sail will be measured in terms of $\beta = 2PA/m$, also know as the sail lightness

number. One can check that, with these definitions, the acceleration for the solar sail in Eq.(2) is written as

$$\begin{aligned} a_x &= \bar{\beta}\cos^2\alpha\cos^2\delta(\rho\cos\alpha\cos\delta + 0.5(1-\rho)), \\ a_y &= \bar{\beta}\cos^2\alpha\cos^2\delta(\rho\sin\alpha\cos\delta), \\ a_z &= \bar{\beta}\cos^2\alpha\cos^2\delta(\rho\sin\delta), \end{aligned} \tag{3}$$

where $\bar{\beta} = \beta(\mu_{sb}\omega^4)^{-1/3}$ is the sail lightness number in normalized units [5].

Some comments on the normalized units

To derive the equations of motion for the AH3BP, we have considered a set of normalized units. Recall that the unit of length is defined as $L = (\mu_{sb}/\mu_{sun})^{1/3}R$, and the unit of time is defined as $T = 1/\omega$. Notice that they both depend on the target asteroid for our mission. In Table 1 we summarize the physical data for different asteroids, as well as the normalized units of distance and time in the normalized Hill problem [5]. We also include the maximum radius of the asteroids in the normalized unit of distance, in order to provide an estimate of the gravity regime for each asteroid (gravity regime is around 3 to 4 times the asteroids' radii). Notice that, for all the asteroids considered, the radius distance varies between 0.001 and 0.005.

Table 1: Relevant parameters for different asteroids

asteroid	μ_{sb} (km^3/s^2)	R (AU)	RADII (km / UD)	UD (km)	UT (day)
Eros	4.463×10^{-4}	1.45	8.42 (2.5×10^{-3})	3265.4	102.2
Vesta	17.8	2.36	265 (1.4×10^{-3})	180782	210
Itokawa	2.1×10^{-9}	1.32	0.165 (3.3×10^{-3})	49.57	88.15
Golevka	$\sim 1.4 \times 10^{-8}$	2.49	0.265 (1.5×10^{-3})	175.96	229.1
Apophis	$\sim 1.8 \times 10^{-9}$	0.92	0.163 (4.9×10^{-3})	32.89	51.4

The normalized sail lightness number is $\bar{\beta} = \beta(\mu_{sb}\omega^4)^{-1/3}$. We recall that $\beta = 2PA/m$, $\omega = \sqrt{\mu_{sun}/R^3}$ and $P = P_0(R_0/R)^2$. Taking this into account, we can rewrite $\bar{\beta}$ as

$$\bar{\beta} = \frac{2P_0R_0^2(A/m)}{\mu_{sun}^{2/3}\mu_{sb}^{1/3}} = K_1(A/m)\mu_{sb}^{-1/3}, \tag{4}$$

where $K_1 \approx 7.8502$ if A is given in m^2 and m in kg. Hence, the value of $\bar{\beta}$ depends on both: $\sigma = (A/m)$, the area-to-mass ratio of the satellite, and μ_{sb}, the gravitational parameter of the small body. We could have the same $\bar{\beta}$ for two completely different missions scenarios. Notice that $\bar{\beta}$ is inversely proportional to $\mu_{sb}^{1/3}$. Hence, for a fixed area-to-mass ratio, the smaller the asteroid the larger the effect of SRP will be.

In Fig. 1 we show the contour levels of the normalized sail lightness number $\bar{\beta}$ as a function of σ and μ_{sb}. As we can see, for small asteroids ($\mu_{sb} \approx 10^{-9}$) and an area-to-mass ratio of a regular spacecraft ($\sigma \approx 0.01$), $\bar{\beta}$ takes values between 50 and 100. In Table 2 we summarize the values of $\bar{\beta}$ for the 5 asteroids in Table 1 and different

[5]The physical parameters have been taken from `http://ssd.jpl.nasa.gov/sbdb.cgi`

area-to-mass rations. As examples, we have taken an estimated area-to-mass ratio for Ikaros ($\sigma \approx 0.63\text{m}^2/\text{kg}$), NanoSail-D2 ($\sigma \approx 2.5\text{m}^2/\text{kg}$), Hayabussa ($\sigma \approx 0.032\text{m}^2/\text{kg}$) and Dawn ($\sigma \approx 0.17\text{m}^2/\text{kg}$). Although Hayabussa and Dawn are not solar sails, they have very large solar panels that could be considered for orbital control [6]. In Table 2 we see again that, around very small asteroids like Itokawa, Golevka and Apophis, SRP is very important, even for a spacecraft like Hayabussa and Dawn.

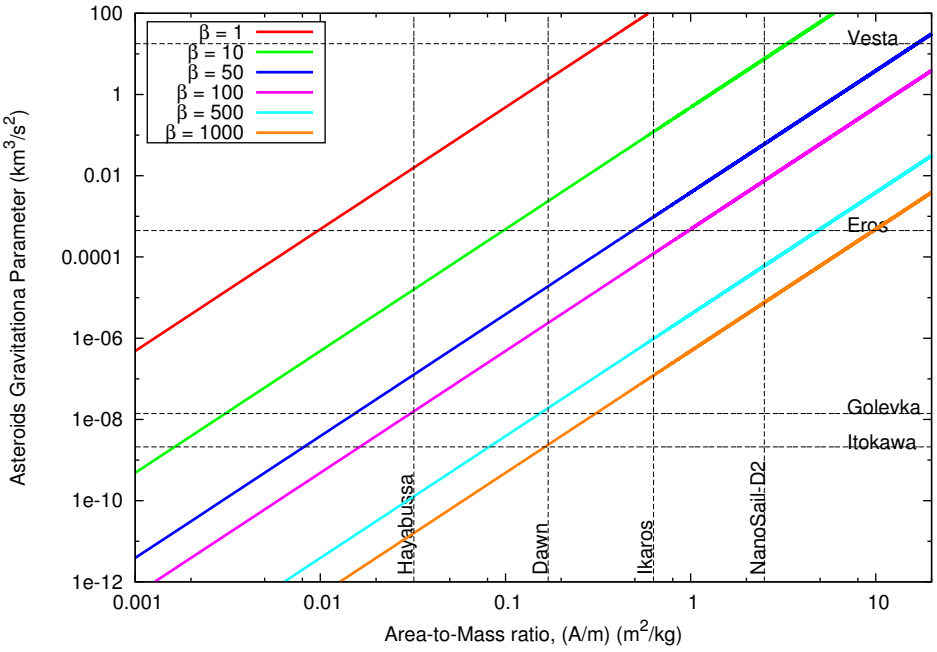

Fig. 1: Contours for $\bar{\beta}$ as a function of (A/m), area-to-mass ratio, and μ_{sb}, the gravitational parameter of the asteroid.

Table 2: Normalized values for $\bar{\beta}$ for different mission configurations

	Ikaros	NanoSail-D2	Hayabussa	Dawn
Eros	64.71	256.809	3.287	17.463
Vesta	1.894	7.51647	0.0962	0.511
Itokawa	3862.02	15325.48	196.166	1042.13
Golevka	2052.0	8142.88	104.228	553.716
Apophis	4065.65	16133.548	206.509	1097.081

Equilibrium Points

The description of the equilibrium points in the AH3BP for a solar sail has already been studied by many authors [7, 8]. Here we give a brief summary of the most important aspects.

It is well known that (x_0, y_0, z_0) is an equilibrium point of the AH3BP for the set of sail parameters $(\bar{\beta}_0, \alpha_0, \delta_0, \rho_0)$

if it satisfies

$$\begin{aligned} 0 &= -\frac{X}{r^3} + 3X + a_x + \bar{\beta}\cos^2\alpha\cos^2\delta(\rho\cos\alpha\cos\delta + 0.5(1-\rho)), \\ 0 &= -\frac{Y}{r^3} + \bar{\beta}\cos^2\alpha\cos^2\delta(\rho\sin\alpha\cos\delta), \\ 0 &= -\frac{Z}{r^3} - Z + \bar{\beta}\cos^2\alpha\cos^2\delta(\rho\sin\delta). \end{aligned} \tag{5}$$

If we neglect the effect of the solar sail ($\bar{\beta} = 0$), we have only two equilibrium points L_1, L_2, symmetrically located around the origin, with coordinates $(\pm 3^{-1/3}, 0, 0)$. When we include SRP and keep the solar sail perpendicular to the Sun-line ($\alpha = \delta = 0$), the position of L_1 and L_2 moves towards the Sun as we increase the value of $\bar{\beta}$. As it can be seen in [9], for $\bar{\beta} > 50$, L_1 is already at more than 16 unit distances from the small body. On the other hand, L_2 gets close to the small body, but still far away from the gravity regime where the shape and spin-rate of the asteroid must be considered. For this reason, from now on we will not consider the dynamics around the displaced L_1 point

Notice that, if $\rho = 0$ (i.e. the only acceleration for the solar sail is given by the absorption), even if we change the sail orientation the equilibrium points will always lie in the x axis, as the effect of changing the sail orientation implies a change on SRP magnitude only, moving the position of equilibria back and forth along the x axis. If $\rho \neq 0$, changing the sail orientation will displace the equilibrium points away from the Sun–asteroid line. For instance, if we tilt the sail vertically w.r.t. the Sun–line (i.e. $\alpha = 0, \delta \neq 0$), we displace the equilibria outside the orbital plane, while if we tilt the sail horizontally w.r.t. the Sun–line (i.e. $\alpha \neq 0, \delta = 0$), we displace the equilibria away from the x axis inside the orbital plane. On the right-hand side of Fig. 2, we have the equilibria on the orbital plane ($Z = 0$) for $\rho = 0.85$, $\bar{\beta} = 10, 20, 30, 50, 75, 100$, $\alpha \in [-\pi/2, \pi/2]$ and $\delta = 0$, where the dashed lines represent values of α between $\pm\pi/4$. We note that: for each $\bar{\beta}$, the equilibrium point closer to the origin corresponds to $\alpha = 0$, and the furthest equilibrium point corresponds to $\alpha = \pm\pi/2$; and the position of the equilibrium points is symmetric with respect to $Y = 0$, hence, if (x_0, y_0, z_0) is a equilibrium point for α_0, then $(x_0, -y_0, z_0)$ is also an equilibrium point for $-\alpha_0$.

Finally, changes on the reflectivity parameter ρ will change the maximal displacement of the "artificial" equilibria with respect to the x-axis. The larger the reflectivity coefficient the more we will be able to displace the equilibrium point from the x axis. This phenomenon can be seen on the left-hand side of Fig. 2, where we have the equilibria on the orbital plane ($Z = 0$) for $\bar{\beta} = 75$, $\alpha \in [-\pi/2, \pi/2]$, $\delta = 0$ and $\rho = 0, 0.15, 0.3, 0.5, 0.75, 0.85$ and 1. Although we just plot the behavior of the equilibrium points for $\delta = 0$, the same effects, for a slightly different scale, are observed when $\alpha = 0$ and $\delta \neq 0$ where the equilibria lie on the $Y = 0$ plane [8].

When we study the stability of these equilibrium points we see that they are all unstable, and that their instability increases as the position of the fixed point comes close to the small body (i.e. as $\bar{\beta}$ increases). This can be seen in Fig. 3, where we plot the maximum absolute value of the eigenvalues $|\lambda|$ versus the x coordinate of the equilibrium points. The equilibria represented in this figure are the same as the ones on Fig. 2.

An important remark is that even for large SRP accelerations, the linear dynamics for all the equilibrium points

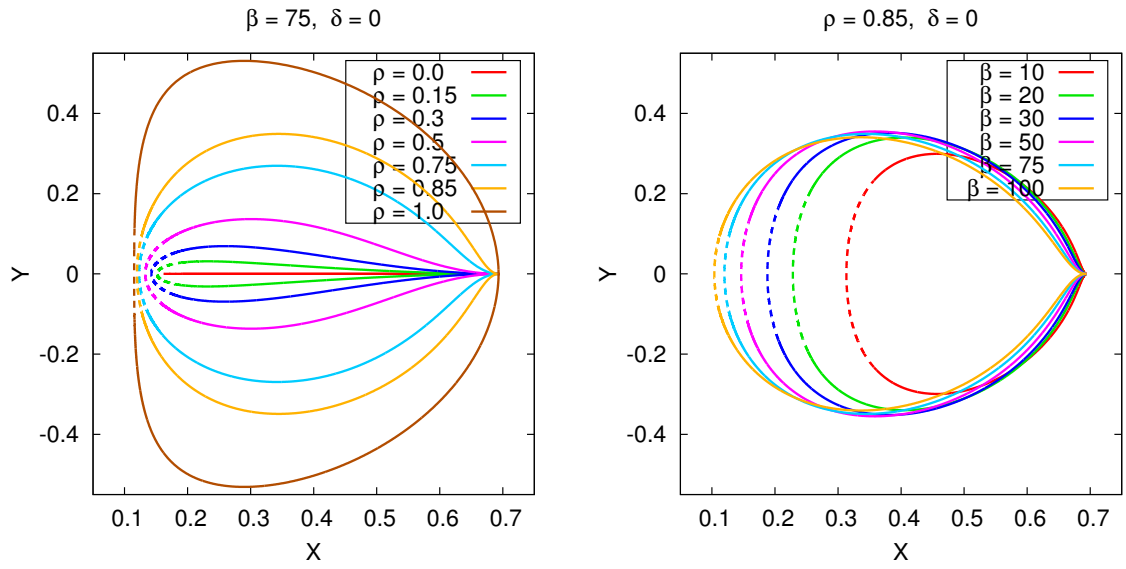

Fig. 2: Equilibrium points on the orbital plane $Z = 0$ (i.e. $\alpha \in [-\pi/2, \pi/2], \delta = 0$) for $\bar{\beta} = 75$ and $\rho = 0, 015, 0.3, 0.5, 0.75, 0.85, 1$ (left), and for $\rho = 0.85$ and $\bar{\beta} = 10, 20, 30, 50, 75, 100$ (right).

has the same structure: saddle×center×center, so the typical families of periodic orbits present in the AH3BP for smaller values of SRP are still present. Namely, the planar and vertical Lyapunov families, as well as the two Halo families, which we will describe in the next section.

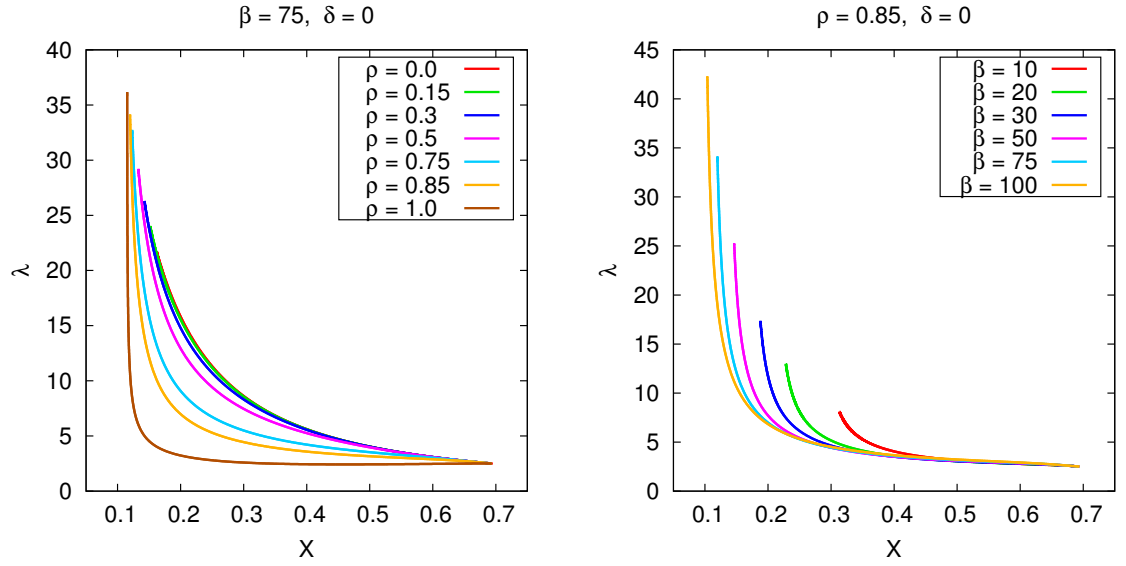

Fig. 3: Maximum absolute value of the eigenvalues, $|\lambda|$, vs the x coordinate of the equilibrium point for: $\bar{\beta} = 75$ and $\rho = 0, 015, 0.3, 0.5, 0.75, 0.85, 1$ (left) and for $\rho = 0.85$ and $\bar{\beta} = 10, 20, 30, 50, 75, 100$ (right).

Periodic Orbits

As mentioned in the previous section, the equilibrium points described are of the type saddle×center×center. Moreover, the system is Hamiltonian for any set of parameters for the sail. Hence, Lyapunov's Center Theorem [10] ensures that, under generic non-resonant conditions, two families of periodic orbits emanate from the fixed point.

Each family is related to one of the two complex pairs of eigenvalues $(\pm \mathtt{i}\omega_1, \pm \mathtt{i}\omega_2)$, and the period of the orbits tends to $2\pi/\omega_i$ when approaching the equilibrium point.

In Fig. 4 we plot for different values of β, ρ, α and δ the difference between the two complex eigenvalues $(\omega_1 - \omega_2)$. When ω_1 and ω_2 coincide, we cannot guarantee the existence of periodic orbits and a more detailed study of this case should be done. Notice in Fig. 4 that this is the case for $\alpha \neq 0, \delta = 0$ (i.e. equilibrium points on the $Z = 0$ plane) where for $\rho \geq 0.5$ we find at least four values for α where this is true. It is not the case for $\alpha = 0, \delta \neq 0$ (i.e. equilibrium points on the $Y = 0$ plane), where $|\omega_1 - \omega_2|$ has a minimum for $\alpha = \delta = 0$, whose value tends to zero as $\bar{\beta}$ increases, but is positive always positive. Still in the $\alpha = 0$ case, the difference between the two center oscillations increases as we move along the family of equilibria.

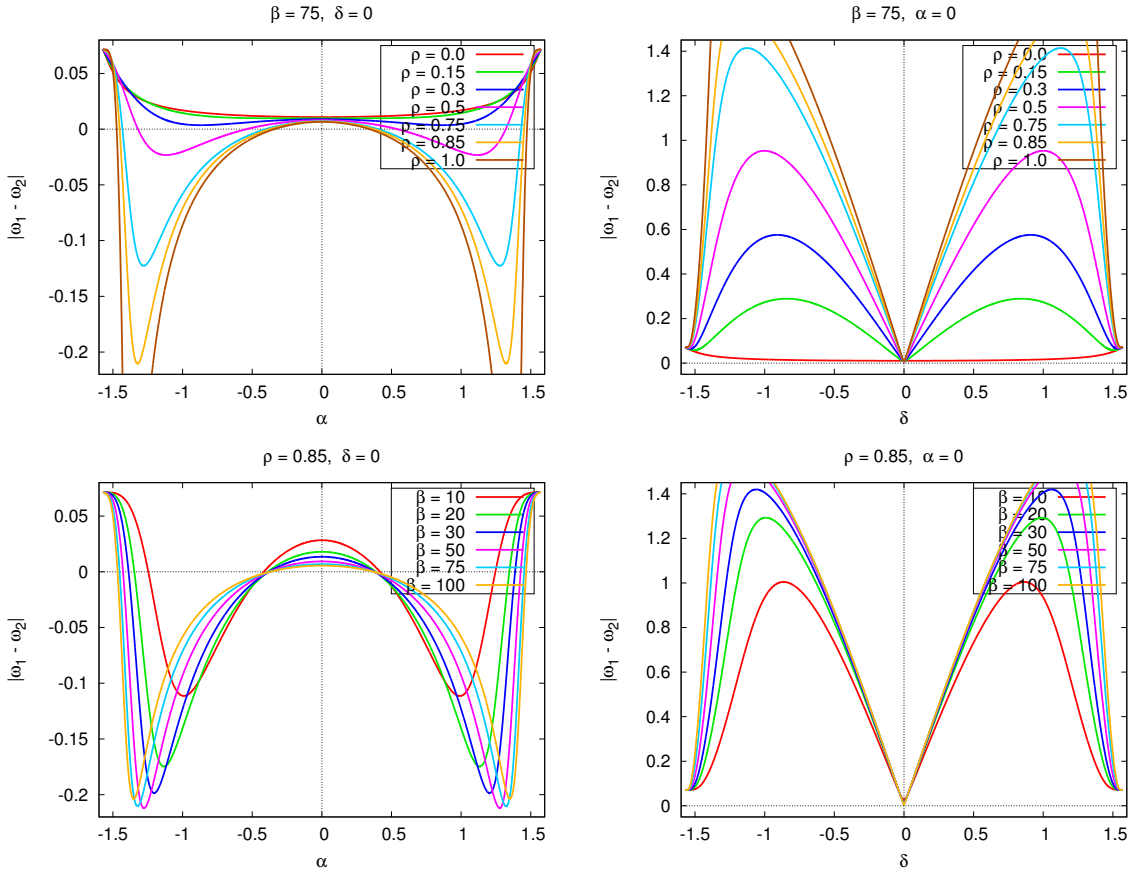

Fig. 4: Difference between the two complex eigenvalues $\omega_1 - \omega_2$ vs α (left) and δ (right) for: $\bar{\beta} = 75$ and $\rho = 0, 015, 0.3, 0.5, 0.75, 0.85, 1$ (top) and for $\rho = 0.85$ and $\bar{\beta} = 10, 20, 30, 50, 75, 100$ (bottom).

Let us describe the families of periodic orbits for $\bar{\beta} = 75$ and their dependence with respect to the sail orientation α, δ and the reflectivity ρ. Taking $\bar{\beta} = 75$ corresponds to a solar sail with an area-to-mass ratio similar to Ikaros on a mission to a middle size asteroid like Eros, or a smaller spacecraft with an area-to-mass ratio like Hayabussa close to smaller asteroids like Golevka (Fig. 1).

To compute the families of periodic orbits for different sail orientations, we will consider appropriate Poicaré sections to ensure the transversality of the flow. For all the computations we have taken as Poincaré section a plane perpendicular to $\{Z = 0\}$ and contains the origin and the equilibrium point for the given sail parameters. Hence, if

(x_0, y_0, z_0) is an equilibrium point for $(\alpha_0, \delta_0, \rho_0)$, then we consider as Poincaré section: $\Gamma = \{x_0 Y - y_0 X = 0\}$. For each family of periodic orbits, we use the linear approximation of the flow around (x_0, y_0, z_0) to compute the first orbit. Then we use a continuation method to compute the rest of orbits of the family, taking the x coordinate of the point on the Poincaré section, Γ, as the continuation parameter.

On the left-hand side of Fig. 5 we plot the continuation diagram of the two families of periodic orbits for $\alpha = \delta = 0$ and $\rho = 0.85$, i.e. the displaced L_2. Each point corresponds to the x and z components of a periodic orbit on the Poincaré section. We have assigned a color to each orbit depending on the linear dynamics around the periodic orbit: blue stands for saddle×center, red stands for saddle×saddle, and green stands for center×center. As we can see, when the planar family crosses a 1:1 resonance, two families of Halo-type orbits are born. As the two center librations of the displaced L_2 point are close a 1:1 resonance ($\mathtt{i}\omega_1 = \mathtt{i}24.1591043, \mathtt{i}\omega_2 = \mathtt{i}24.1522099$) the two Halo orbits bifurcate from the planar family very close to the equilibrium point. Their bifurcation takes place at the rightmost point of Fig. 5 left. At the scale of this Figure, it is indistinguishable from the birth of the planar and vertical Lyapunov families. On the right-hand side of Fig. 5 we plot the variation of the *stability parameters*[6], $s_{1,2}$, along the family.

Both the planar and vertical families of periodic orbits are linearly unstable. The planar family is center×saddle close the equilibrium point, but as it crosses the 1:1 resonance, a bifurcation occurs and the orbits become saddle×saddle. The Halo orbits that are born inherit the center×saddle dynamics at first, but as we move along the family they become stable. Nevertheless, notice that, for each family, instability decreases as we reach the terminating orbits.

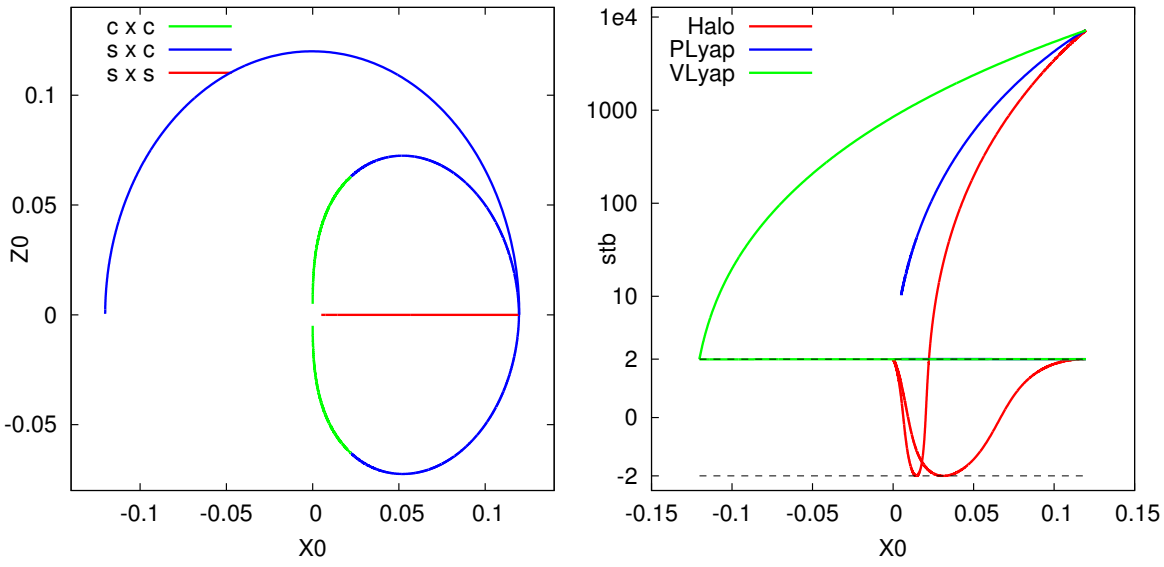

Fig. 5: For $\bar{\beta} = 75$, $\alpha = \delta = 0$ and $\rho = 0.85$. Left: continuation diagram of the families of periodic orbits, Right: variation of the stability parameters for the orbits on the family.

In Fig. 6 we show the X, Y, Z projection for these three type of orbits. Form left to right we have the Planar,

[6]The *stability parameters* of a periodic orbit are defined as $s_i = \lambda_i + \lambda_i^{-1}$, for $i = 1, 2$, where λ_i belongs to the spectra of the monodromy matrix associated to a periodic orbit. As the system is autonomous and Hamiltonian with two degrees of freedom, if M is the monodromy matrix of a periodic orbit, $\mathrm{Spec}(M) = \{1, 1, \lambda_1, \lambda_1^{-1}, \lambda_2, \lambda_2^{-1}\}$.

Vertical and Halo type orbits. We observe that the orbits on the planar family are on the orbital plane ($Z = 0$), and have a boomerang shape, that gets more elongated as we move along the family, and leaves the asteroid in the middle. The orbits on the vertical family have the familiar eight shape, spending half of their orbital period above the orbital plane, and as we move along the family the orbits loose vertical displacement, to become almost planar close to their terminator. Finally, the two families of Halo orbits are almost circular and remain on the shadow side of the asteroid.

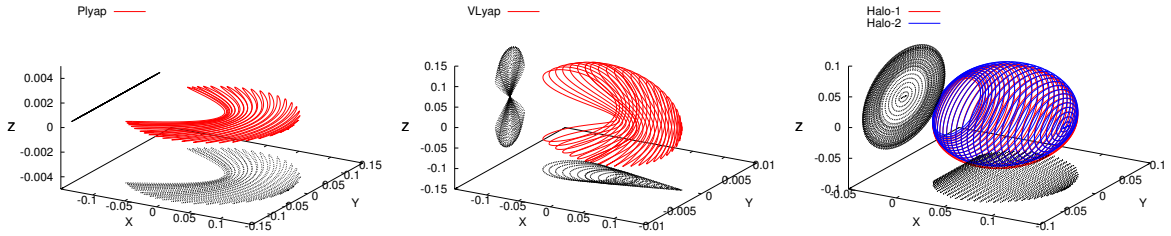

Fig. 6: Family of periodic orbits for $\bar{\beta} = 75$, $\alpha = \delta = 0$ and $\rho = 0.85$. From left to right: Planar Lyapunov orbits, Vertical Lyapunov orbits and Halo-type orbits

As it happened with the equilibrium points, changing the sail orientation allows us to displace these families of periodic orbits. Small changes on the sail orientation will not change the general structure of the families, and we will still find the three kind of periodic orbits (Planar, Vertical and Halo). If we take $\alpha = 0$ and $\delta \neq 0$, we will displace the families of periodic orbits above the orbital plane. As it happened in [11], there is a symmetry breaking on the equations for $\delta \neq 0$, which changes the way in which these orbits relate. The planar family of orbits emanating from the fixed point starts almost planar, but as we move along the family, these orbits start to gain vertical amplitude in such a way that they can be considered Halo orbits. Nevertheless, the planar orbits still exist, and can be found by continuing planar orbits for $\delta = 0$ with respect to δ. These orbits still have the boomerang shape and are slightly inclined with respect to the orbital plane. The orbits in the vertical family still have an eight shape, but the loops are slightly asymmetric. If we take $\delta = 0$ and $\alpha \neq 0$, we displace the families of periodic orbits sideways with respect to the Sun–asteroid line. The overall structure is the same as for $\alpha = \delta = 0$, i.e. we have the planar and vertical families of orbits, and at the 1:1 resonance between the planar and vertical frequencies the Halo orbits appear. Planar orbits still have the boomerang shape, orbits in the vertical family have an eight shape and Halo orbits are almost circular and perpendicular to the orbital plane. The main difference is that they are tilted, but still approach the small body as we move along the family.

We must mention that, for large changes of the sail orientation, the nature of the families periodic orbits that we have just described can drastically change. For instance, for $|\alpha| > 0.5$, we have observed that, if we continue along the planar family of orbits, we do not cross a 1:1 resonance and the Halo-type orbits do not appear. A study of these phenomena is in progress.

In Fig. 7 we show the X, Y, Z projection of the three type of orbits for $\alpha = 0.2$rad, $\delta = 0$rad and $\rho = 0.85$. We can see how the orbits have the same shape as in Fig. 6 but they are tilted with respect to the asteroid–equilibrium

point line. In Fig. 8 we show the X, Y, Z projection of the three type of orbits for $\alpha = 0$rad, $\delta = 0.02$rad and $\rho = 0.85$. Observe that here the orbits are tilted above the orbital plane.

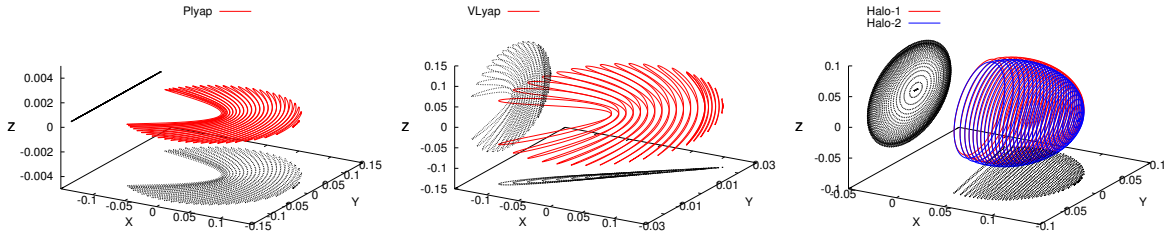

Fig. 7: Family of periodic orbits for $\bar{\beta} = 75$, $\alpha = 0.2, \delta = 0$ and $\rho = 0.85$. From left to right: Displaced planar Lyapunov orbits, displaced vertical Lyapunov orbits and displaced Halo-type orbits

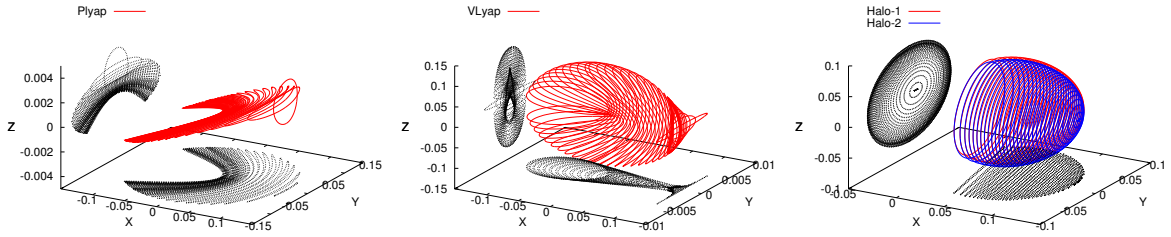

Fig. 8: Family of periodic orbits for $\bar{\beta} = 75$, $\alpha 0, \delta = 0.02$ and $\rho = 0.85$. From left to right: Displaced planar Lyapunov orbits, displaced vertical Lyapunov orbits and displaced Halo-type orbits

Finally, a change on the reflectivity parameter ρ, will also displace these families of periodic orbits. If we look at Eq. (3), we notice that if we change ρ we are changing the direction of a_{SRP}. Hence, we can think of a change in ρ as a change in the sail orientation. In Fig. 9 we plot several planar and vertical orbits from $\bar{\beta} = 75, \alpha = 0.2, \delta = 0$ and different values of ρ. As we can see, the effect of varying the reflectivity is similar to the one obtained varying the sail orientation. The periodic orbits are tilted towards the Sun–asteroid line as ρ tends to 0.

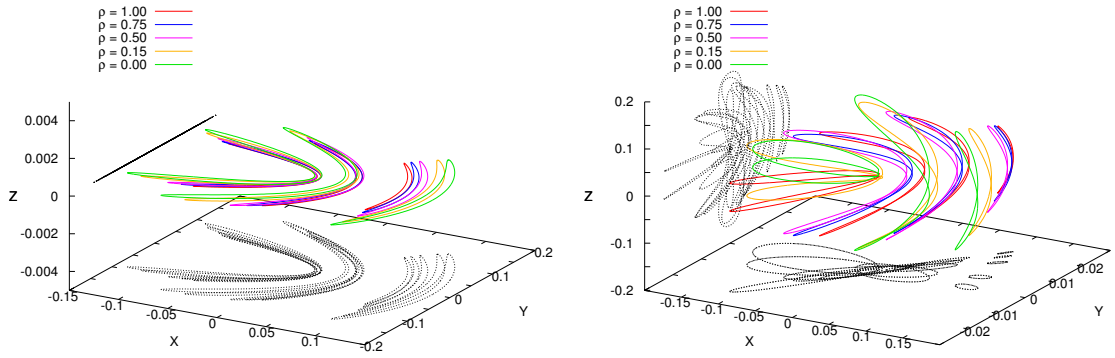

Fig. 9: Periodic orbits for $\bar{\beta} = 75$, $\alpha 0.2, \delta = 0$ and $\rho = 0, 0.15, 0.5, 0.75$ and 1. Left: displaced planar Lyapunov orbits and right: displaced vertical Lyapunov orbits

Some comments on the Terminator Orbits

If we were to plan a mission to an asteroid with a solar sail, there are a several restrictions that must be taken into account. For instance: orbiting close to the asteroid to allow more detailed scientific observations; keeping the solar sail almost perpendicular to the SRP to magnify the performance of the sail; and being able to observe the day side of the asteroid.

As we know, L_2 and "artificially" displaced equilibrium points are on the shadow side of the asteroid, which could compromise an observational mission [8]. On the other hand, some of the periodic orbits that we have just described spend a part of their orbital period on the day side of the asteroid, and could be used for observational missions at asteroids. This is the case for the terminator orbits from the planar Lyapunov and vertical Lyapunov families. In Fig. 10 we show one orbit of each family that spends some time on the day side of the asteroids.

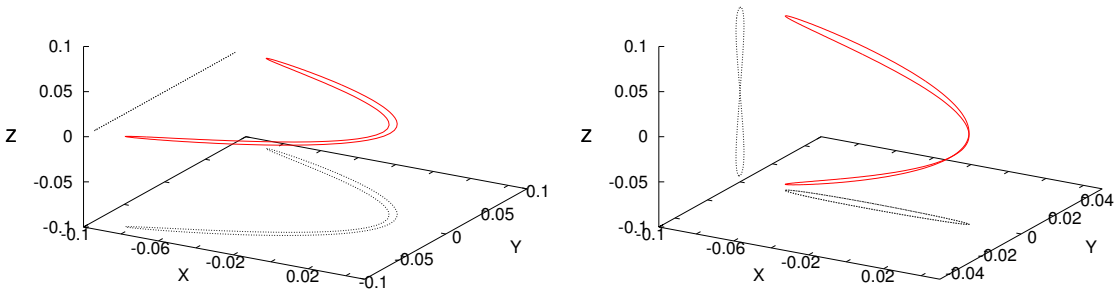

Fig. 10: A planar Lyapunov (left) and a vertical Lyapunov (right) periodic orbit on the terminator family that spends more that half of its period in the day side of the asteroid

We have done some preliminary tests on the feasibility of these orbits, checking the maximum and minimum distance to the center of the asteroid, as well as the amount of time each orbit spends on the day side of the asteroid. We have seen that, for $\bar{\beta} = 75, \rho = 0.85$ and $\alpha = \delta = 0$, we can find terminator orbits in the planar and vertical Lyapunov families that have the closest approach with the small body at a distance of 0.01 or less normalized units (that correspond to 4 radii in the case of Eros), and a maximum distance from the asteroid of ≈ 0.12 normalized units ($\approx$48 radii for Eros). Finally, the terminator planar Lyapunov orbits spend more than 90% of their orbital period on the day side, and their average period is of ≈ 0.15 (around 15 days for Eros). The terminator vertical Lyapunov orbits spend around 70% of their orbital period on the day side, and have an average period of ≈ 0.11 (around 11 days for Eros).

Conclusions and Future Work

In this paper we have considered the Augmented H3BP as a model for the dynamics of a solar sail close to an asteroid, and we have described some aspects of the natural dynamics of the system for the different parameters defining the performance of the solar sail and its orientation. We have computed fixed points and families of periodic orbits. Some of these periodic orbits, such as the terminator planar and vertical Lyapunov orbits, spend most of their orbital period on the day side of the asteroid and could be interesting for observational missions to

asteroids. Nevertheless, these orbits are unstable and require control strategies. A study on the controllability of these orbits is progress.

There are many aspects on the dynamics of the Augmented H3BP that still need to be addressed. In the near future, we plan to do a complete study on the non-linear dynamics around the equilibrium points. We are currently performing a reduction to the center manifold, to be able to have a complete description of the periodic and quasi-periodic motion. Moreover, the stable and unstable manifolds of the equilibrium points and periodic orbits, can be interesting for low-energy transfers or approximation maneuvers to the surface of the asteroid. Finally, it is known that some asteroids follow very eccentric orbits around the Sun. The variation of the distance to the Sun also plays an important role in the dynamics of the system [9], and should be taken into account.

Acknowledgments

A.F. and A.J. have been supported by the Spanish grant MTM2009-09723 and the Catalan grant 2009SGR67. J.M.M. has been supported by the Spanish grants MTM2011-26995-C02-01, MTM2010-16425, and the Catalan grant 2009SGR410.

References

[1] D.J. Scheeres. *Orbital Motion in Strongly Perturbed Environments: Applications to Asteroid, Comet and Planetary Satellite Orbiters*. Astronautical Engineering. Springer, 2012.

[2] C.R. McInnes. *Solar Sailing: Technology, Dynamics and Mission Applications*. Springer-Praxis, 1999.

[3] B. Dachwald, W. Seboldt, M. Macdonald, G. Mengali, A.A. Quarta, C.R. McInnes, L. Rios-Reyes, D.J. Scheeres, B. Wie, M. Görlich, et al. "Potential Solar Sail Degradation Effects on Trajectory and Attitude Control". In *AIAA Guidance, Navigation, and Control Conference and Exhibit*, volume 6172, 2005.

[4] D. Scheeres and F. Marzar. "Spacecraft Dynamics in the Vicinity of a Comet". *The Journal of the Astronautical Science*, 50(1):35–52, January–March 2002.

[5] Y. Katherine and B. Villac. "Periodic Orbits Families in the Hill's Three-Body Problem with Solar Radiation Pressure". In *Advances in the Astronautical Sciences Series*, volume 136, San Diego, California, 2010.

[6] B. Villac, G. Ribalta, A. Farrés, À. Jorba, and J-M. Mondelo. "Using Solar Arrays for Orbital Control Near Small Bodies. Trade-offs characterization.". In *AIAA/AAS Astrodynamics Specialist Conference*, Minneapolis, Minnesota, 2012.

[7] E. Morrow, D. Scheeres, and D. Lubin. "Solar Sail Orbit Operations at Asteroids". *Journal of Spacecraft and Rockets*, 38(2):279–286, March–April 2001.

[8] M. Giancotti and R. Funase. "Solar Sail Equilibrium Positions and Transfer Trajectories close to a Trojan Asteroid". In *Proceedings of the 63rd International Astronautical Congress*, 2012.

[9] A. Farrés and À. Jorba. "Orbital dynamics of a solar sail near L1 and L2 in the Elliptic Hill problem". In *Proceedings of the 63rd International Astronautical Congress*. IAF, 2012.

[10] K.R. Meyer and G.R. Hall. *Introduction to Hamiltonian Dynamical Systems and the N-Body Problem*. Springer, New York, 1992.

[11] A. Farrés and À. Jorba. Periodic and quasi-periodic motions of a solar sail around the family SL_1 on the Sun-Earth system. *Celestial Mechanics and Dynamical Astronomy*, 107:233–253, 2010.